PROBING THE UNIQUE MORPHOLOGY AND PLASMA CONDITIONS OF W49B WITH *CHANDRA*

Supernova remnants (SNRs) are a diverse class of objects that play an essential role in the dynamics of the interstellar medium (ISM) and that produce and distribute most of the metals in the Universe (Fukugita & Peebles 2004). Since its launch, the *Chandra* X-ray Telescope has observed over one-hundred SNRs in the Milky Way and many more in the Local Group. The sub-arcsecond spatial resolution and spectro-imaging capabilities of the *Chandra* X-ray Telescope facilitate detailed studies of the metal-rich ejecta of SNRs and their interaction with the ISM as they expand.

I. Background

W49B (G43.3−0.2) is the brighest ejecta-dominated SNR in X-rays ($L_X \sim 10^{38}$ erg s^{-1}; Immler & Kuntz 2005), and it has the highest surface brightnesses at 1 GHz of all Galactic sources (Moffett & Reynolds 1994). Radio maps show the source has a prominent shell ≈4' in diameter, yet it has a center-filled morphology in the X-rays. In fact, high-resolution *Chandra* X-ray images (see insets of Figure 1) show the emission is elongated in a centrally bright, iron-rich bar and has two plumes at its eastern and western edges. The global X-ray spectrum of W49B (Fig. 1) has strong emission lines from He-like and H-like ions of Si, S, Ar, Ca, and Fe. These metals have supersolar abundances (indicating an ejecta origin), and the spectra are typically modeled as two plasmas in collisional ionization equilibrium.

Previous X-ray studies have demonstrated that W49B has several unique morphological and spectral features which are not found in other galactic SNRs. Foremost, W49B is the *only* galactic SNR with large-scale segregation of its elements (Lopez et al. 2009, 2011): the Fe XXV is missing from the Eastern half of the SNR, while the lower-Z ions are more spatially homogeneous (see Figure 1). Secondly, the X-ray spectrum is suggestive of rapid cooling which is uncommon in SNRs: it has a strong radiative recombination continuum from H-like Fe (Ozawa et al. 2009), and electron temperatures derived from the bremsstrahlung shape are systematically lower than those estimated using He-like and H-like line ratios (e.g., Kawasaki et al. 2005). Finally, W49B is the only core-collapse SNR to date with detected He-like lines from the heavy elements chromium Cr and manganese Mn (Hwang et al. 2000, Miceli et al. 2006). *These unique properties of W49B make it an exciting testbed for explosion, dynamical, and plasma models of SNRs.*

Several outstanding questions remain regarding the physical origin of W49B's surprising traits: is the complex morphology of W49B due to its explosive origin or an inhomogeneous environment? What is the ionization state of the plasma across the source, and why is the plasma cooling rapidly? What do the morphology and abundances of Cr and Mn reveal about the progenitor of W49B?

II. Proposed Observations

To aid in answering these questions, we propose a deep, 220-ks *Chandra* ACIS-S3 observation of W49B. The source was observed previously in 2000 for 55 ks with the ACIS-S3 chip in Timed-Exposure Faint Mode (ObsID=117); after background subtraction, $\approx 2.4 \times 10^5$ total counts were detected in the full-band (0.5–8.0 keV) in the $4'$ diamater of the SNR (Lopez et al. 2009). Therefore, we anticipate $\sim 10^6$ net counts in the full band in our proposed program. As demonstrated below, these data will facilitate morphological and spatially-resolved spectral analyses that will elucidate the physical conditions and nature of W49B. Only *Chandra* has the spatial and spectral resolution necessary to facilitate the morphological and spectro-imaging analyses proposed here.

III. Proposed Analysis & Science Goals

• **Probing Explosion Vs. Environment Effects**: The explosive origin of W49B has been debated in previous X-ray studies. Based on the abundance ratios from fits to the integrated

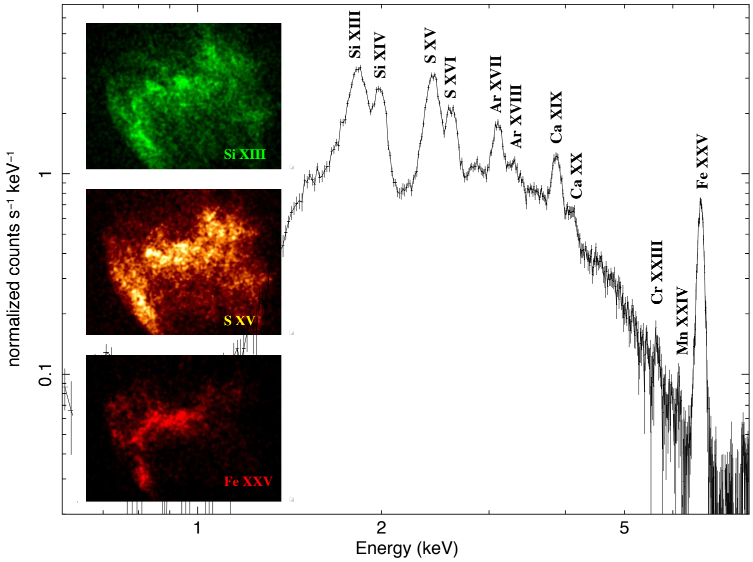

Figure 1: Integrated spectrum from the 55 ks *Chandra* ACIS observation of W49B (Lopez et al. 2009). The spectrum has numerous prominent emission lines as well as a strong bremsstrahlung continuum. Since W49B is in the Galactic plane, it is highly absorbed (with $N_H \approx 5 \times 10^{22}$ cm^{-2}), attenuating the soft X-rays. Inset images show the morphologies of Si XIII, S XV, and Fe XXV. Fe XXV emission is weak in the Eastern region of W49B, while the Si and S are more homogeneously distributed.

ASCA spectrum, Hwang et al. (2000) suggested W49B likely had a Type Ia progenitor. However, follow-up spectral analyses of 23 distinct regions with *XMM* data showed that the abundance ratios vary dramatically (by up to factors of 4) with position, and the median values are consistent with model predictions for an asymmetric core-collapse (CC) SN (Lopez et al. 2009). This result underscores *the necessity for a systematic, spatially-resolved analysis of distinct regions in W49B.*

To aid in understanding the complex morphology of W49B, we developed and applied three mathematical tools to quantify morphological properties (Lopez et al. 2009a): wavelet-transform analysis to measure substructure scale and location, two-point correlation to quantify chemical segregation, and a power-ratio method (a multipole expansion) to probe large-scale symmetry. When applied to the *Chandra* X-ray line images of W49B, we found that the Fe XXV morphology is statistically more asymmetric, more segregated, and has 25% larger substructures than lower-Z elements. These results contrast those of other SNRs: similar analyses of eight other galactic SNRs showed all their X-ray line morphologies were the same, with <6% differences. Thus, *W49B is the only known remnant with large-scale segregation of its nucleosynthetic products.*

Two potential scenarios may account for the barrel shape of W49B (see insets of Fig. 1): it could be due to a bipolar/jet-driven explosion of a massive star, or it may be the result of an inhomogeneous ISM around a spherically-symmetric SN. The latter explanation is appealing because it applies to other sources as well (e.g., G292.0+1.8: Park et al. 2004). Unfortunately, this scenario would require unrealistic ejecta masses in W49B (Keohane et al. 2007). A bipolar origin is consistent with the abundance ratios given from the *XMM* spectral fits, and it may account for the anisotropic distribution of iron since heavy elements are preferentially ejected along the polar axis of the progenitor in these explosions (Mazzali et al. 2001, Ramirez-Ruiz & MacFadyen 2010). However, the predicted rate of such events is estimated to be low (∼1 per 1000–10000 years per galaxy: Lopez et al. 2011).

To constrain explosion vs. environment effects, we propose to extract and model X-ray spectra systematically from a "grid" across W49B (see Fig. 2) to map column density, electron temperature, metal abundances, and emission measure. In these maps, significant evironment effects would be evident through e.g., gradients in temperature or column density. We will also quantify the morphological properties of the metals using the methods described above, and we will test how the local and global ion distributions depend on the thermodynamic properties given by the spectral fits. Additionally, we will compare abundance ratios and metal masses (estimated from the emission measures) to theoretical model predictions for spherical and aspherical CC SNe to ascertain the progenitor of W49B. *If these detailed analyses confirm its bipolar CC origin, then W49B would be the only local analogue known of gamma-ray bursts, the highest-energy explosions in the universe.*

• **Localizing the Over-Ionized Plasma in W49B**: Recently, evidence has emerged that the plasma in W49B may be "over-ionized". Using integrated *ASCA* spectra, Kawasaki et al. (2005) measured the intensity ratios of H-like to He-like lines of Ar and Ca, and they found ionization temperatures ($kT_{\rm z}$ ∼2.5 keV) much higher than those derived from the bremsstrahlung continuum shape ($kT_{\rm e}$ ∼1.8 keV). Furthermore, observations of W49B with *Suzaku* revealed a "bump" at ∼9 keV which corresponds to the electron binding energy of Fe, suggesting the feature is the result of a radiative recombination continuum (RRC) of Fe (Ozawa et al. 2009). Based on modeling of this feature, these authors find the Fe ionzation temperatures $kT_{\rm z}$ ∼2.7 keV, which is also $\gg kT_{\rm e}$.

Miceli et al. (2010) attempted to spatially localize the over-ionized plasma by analyzing the hardness-ratio map from the *XMM* observation of W49B. They found evidence for the over-ionized plasma in the central and Western regions of W49B, while the Eastern part of the SNR appears to be in ionization equilibrium. Thus, *the ionization state varies across W49B, and a deeper observation is critical to facilitate a detailed, spatially-resolved analysis of the plasma conditions.*

The physical origin of the over-ionization remains uncertain, particularly since plasmas of young SNRs are generally under-ionized. Over-ionization is a signature of rapid cooling of the ejecta. One scenario where such cooling can occur is if ejecta interact with an inhomogeneous ISM, it may produce a reflected shock that efficiently heats and ionizes the metals; subsequently, the ejecta expand adiabatically and cool (e.g., Yamaguchi et al. 2009). Another possibility is the hot interior of the SNR cools rapidly via thermal conduction to the cool exterior (e.g., Zhou et al. 2011).

To probe the physical origin of this over-ionization, we propose to spatially identify the over-ionized plasma and to describe systematically the plasma conditions in W49B. We will estimate the ionization temperatures $kT_{\rm z}$ from intensity ratios of the H-like to He-like lines of Si and S (and of Ar and Ca, where signal allows). These values will be compared with $kT_{\rm e}$ derived from spectral fits to the bremsstrahlung continuum. Using these results, we will produce maps of the level of ionization across the source, and we will identify regions in ionization equilibrium and over-ionization. Given the substantial variation in $kT_{\rm e}$ across W49B ($kT_{\rm e}$ ≈1.8–3.7 keV: Lopez et al. 2009), this spatially-resolved analysis is necessary to obtain an accurate assessment of the plasma.

The trends in temperature and ionization state can be compared to those expected in the different cooling scenarios. For example, if the plasma is cooling via thermal conduction, then there should be a temperature gradient with radius (with hotter temperatures at small radii).

• **Constraining the Morphology and Abundance of Chromium and Manganese**: *W49B is the only core-collapse SNR with X-ray emission lines detected of chromium Cr and manganese Mn.* He-like Cr (with line energy 5.69 keV) and Mn (with line energy 6.17 keV) were first detected in the integrated *ASCA* spectra from W49B by Hwang et al. (2000). Hints of these lines are evident in the 55-ks integrated *Chandra* X-ray spectrum. Like iron, Cr and Mn are products of explosive silicon burning, whereas the other X-ray bright metals (e.g., Si, S, Ar, and Ca) are products primarily of explosive oxygen burning (Woosley, Heger, & Weaver 2002).

We propose to quantify the morphologies of Cr and Mn and the other metals in W49B using the mathematical methods we developed previously (Lopez et al. 2009). We will measure the spatial distributions and substructure properties of Cr and Mn, and we will test statistically whether their morphologies trace the anomalous distribution of Fe in W49B.

Additionally, as a means to understand why other SNRs do not have strong Cr and Mn emission, we will examine the thermodynamic conditions of the plasma in locations with and without Cr and Mn emission. We will also model the Cr and Mn abundances in our spectral fits, and compare the results to theoretical predictions from CC SN models to constrain better the progenitor.

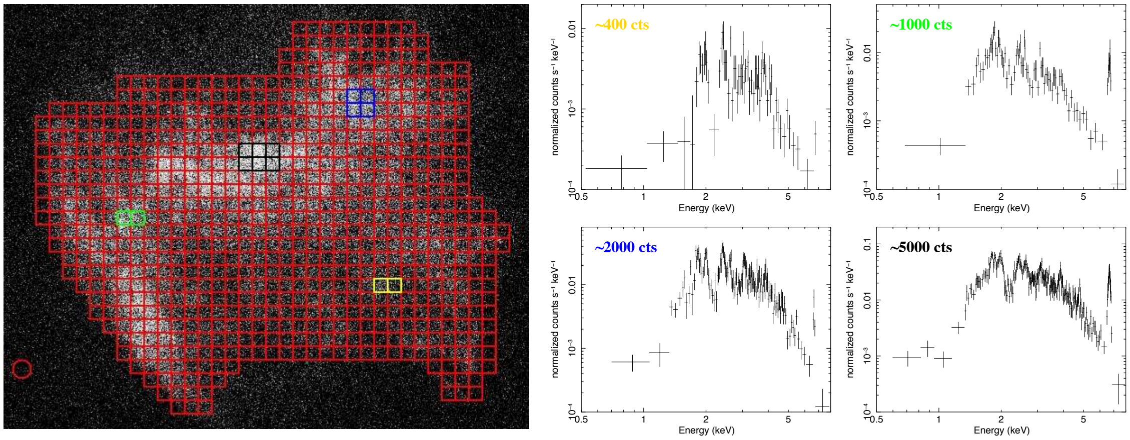

Figure 2: *Left*: Saturated full-band (0.5–8.0 keV) image of W49B from 55-ks ACIS-S observation with $7.5'' \times 7.5''$ boxes overplotted. With a 220-ks observation, ≈94% of the regions will have >400 net counts in the full-band. *Right*: Example background-subtracted spectra from four locations in W49B (corresponding to the colored regions in the image) to demonstrate the quality of spectra with 400, 1000, 2000, and 5000 counts. The 400-count spectrum has 2σ error bars, and the others have 3σ error bars.

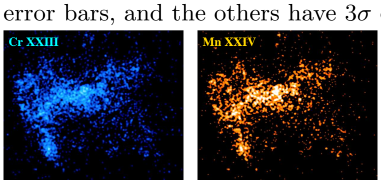

Figure 3: Simulated images of Cr XXIII and Mn XXIV (smoothed with a Gaussian kernel of σ=5 pixels), assuming the metals trace the morphology of Fe XXV. Images have counts set to those expected for the 220-ks observation (see §IV).

IV. Feasibility

Based on the count rate from the 55-ks ACIS-S3 observation of W49B, we anticipate $\sim 10^6$ net counts in the full band (0.5–8.0 keV) in a 220-ks observation. We have selected this integration time to ensure we have >400 net full-band counts in almost all (≈94%) of the $7.5'' \times 7.5''$ regions in Figure 2 (the median size of individual emitting substructures in W49B: Lopez et al. 2009). We estimate that a minimum of 400 full-band counts are necessary to fit the bremsstrahlung shape and the line emission accurately (see Fig. 2) so that we can map e.g. temperatures across W49B.

Fig. 2 also gives example spectra for regions with 1000, 2000, and 5000 counts, to demonstrate how many counts are necessary to discern specific features. The He-like and H-like lines of Si and S begin to be distinguishable with 1000 counts, and they can be readily apparent with 2000 counts. Therefore, we expect to be able to assess the ionization state in 50–100 regions across W49B.

In the 55-ks observation of W49B, ≈1200 net counts and ≈700 net counts were detected in the energy bands of He-like Cr (≈5.6–5.8 keV) and Mn (≈6.07–6.27 keV), respectively. Therefore, we anticipate ≈4800 net counts and ≈2800 net counts from these energy bands in our deep observation. These values will be sufficient to assess the spatial distribution of these metals: Figure 3 gives the simulated images of Cr XXIII and Mn XXIV (assuming the morphology traces the Fe XXV), with total net counts set to those expected in the 220-ks observation.

The collaboration behind this proposal includes experienced X-ray observers as well as high-energy theorists to assist in the physical modeling and interpretation of results.

References: • Fukugita & Peebles 2004, ApJ, 616, 643 • Hwang et al. 2000, ApJ, 532, 970 • Immler & Kuntz 2005, ApJ, 632, L99 • Kawasaki et al. 2005, ApJ, 631, 935 • Keohane et al. 2007, ApJ, 654, 938 • Lopez et al. 2009, ApJ, 691, 875 • Lopez et al. 2011, ApJ, in press, arXiv: 1011.0731 • Mazzali et al. 2001, ApJ, 559, 1047 • Miceli et al. 2006, A&A, 453, 567 • Miceli et al. 2010, A&A, 514, L2 • Moffett & Reynolds 1994, 437, 705 • Ozawa et al. 2009, ApJL, 706, L71 • Park et al. 2004, ApJL, 602, L33 • Ramirez-Ruiz & MacFadyen 2010, ApJ, 716, 1028 • Woosley, Heger, & Weaver, 2002, RvMP, 74, 1015 • Yamaguchi et al. 2009, ApJL, 705, L6 • Zhou et al. 2011, MNRAS in press, arXiv: 1103.2290